polymers

MDPI

Article

Light-Activated Elongation/Shortening and Twisting of a Nematic Elastomer Balloon

Lin Zhou [1], Yujie Wang [2] and Kai Li [2,*]

[1] School of Mechanical and Electrical Engineering, Anhui Jianzhu University, Hefei 230601, China; zhoulin@ahjzu.edu.cn
[2] Department of Civil Engineering, Anhui Jianzhu University, Hefei 230601, China; yjwang_@outlook.com
* Correspondence: kli@ahjzu.edu.cn

Abstract: Nematic elastomer balloons with inflation-induced axial contraction and shear/torsion effect can be used as actuators for soft robots, artificial muscles, and biomedical instruments. The nematic elastomer can also generate drastic shape changes under illumination, and thus light can be utilized to activate the deformation of nematic elastomer balloons with huge advantages of being accurate, fast, untethered, and environmentally sustainable without chemical byproducts. To explore light-activated deformation behaviors of the balloon, a phenomenological relationship between light intensity and material parameters describing polymer backbone anisotropy is proposed from experiments, and a theoretical model of an optically-responsive nematic elastomer balloon is established based on the nematic elastomer theory. Various light-activated elongation/shortening and twisting behaviors in the cases of free-standing and axial-loading are presented and their mechanisms are elucidated. The light intensity and initial mesogen angle have great influences on the light-activated deformations including the radius, length, shearing angle and mesogen angle. Light can be easily controlled to trigger rich deformation processes, including elongation/shortening and torsion. The results of this paper are expected to promote the understanding of the light-activated deformation behaviors of the nematic elastomer balloon, and the applications in light-activated actuators and machines.

Keywords: nematic elastomer; balloon; optically-responsive; contraction; twisting

Citation: Zhou, L.; Wang, Y.; Li, K. Light-Activated Elongation/Shortening and Twisting of a Nematic Elastomer Balloon. *Polymers* **2022**, *14*, 1249. https://doi.org/10.3390/polym14061249

Academic Editor: Marcin Masłowski

Received: 18 February 2022
Accepted: 17 March 2022
Published: 20 March 2022

1. Introduction

Nematic elastomer represents a new type of polymer composite intelligent material, which is moderately crosslinked with non-crosslinked liquid crystal polymer and exhibits elasticity during the transition from isotropic state to liquid crystal state [1]. The mechanical behaviors are determined by the stretch of polymer chains as well as rotation of liquid crystal mesogens within it [2]. The self-organization of liquid crystal systems and the flexibility brought by elasticity of the polymer network allow large and reversible anisotropic dimensional changes under external stimulations. The nematic elastomer bears the most abundant mechanical properties and has been studied extensively [3–7]. Recently, nematic elastomer has been widely used in the fields of micro/nano devices, sensors and actuators [8–14].

Nematic elastomer tubes or balloons are often used to build artificial muscles which can be utilized in robotic arms, prosthetics, medical robots [15–18]. Many intriguing phenomena associated with large deformation of balloons have been observed and intensively studied in the past several decades [19–22]. He et al. [15] experimentally analyzed the anomalous inflation phenomenon of the cylindrical nematic elastomer balloons when subjected to an additional axial load and adopted a theory based on the quasiconvex free energy to understand the inflation behaviors. Theoretical research on the inflation-induced torsion of a cylindrical nematic elastomer balloon under the combined action of axial loading and

inflating pressure was carried out by Li et al. [23]. The inflation process of the nematic elastomer balloon shows various performances in the cases of different axial tensions. Similar to the routine balloon, a bifurcation condition is valid by Maxwell's equal-area rule and the localized bulge can take place in the inflating process [24–26]. It was found that the existence of disconnected solution branches and the bifurcation may undergo a jump from one branch to another, which is accompanied with the director reorientation similar to the uniaxial nematic elastomers [27] or bent nematic liquid crystal elastomers [28,29].

Through integrating photoisomerizable molecules into nematic elastomer, large and reversible deformations of the nematic elastomer composite material can be induced optically [1,30–37]. The sufficient illumination can change the nematic order through isotropic–nematic phase transition and produce reorientation of the liquid crystal mesogens. The isotropic-to-nematic phase transition provides nematic elastomer with an unusual soft elasticity and generates shape changes under light illumination [38–42]. Recently, experiments were conducted on a range of different photoactive nematic elastomers and focused on describing the specific actuation modes such as periodic behavior and bending/uniaxial contraction effects of nematic films [43–46]. In order to explain its behaviors and development for photo-induced deformation, many kinds of theoretical models have been proposed [1,43,47]. Bai et al. [48] explored the mechanical behavior of a photoactive nematic elastomer under both light intensity and external force. He et al. [49] conducted the theory of uniaxial tension of a nematic elastomer film with different initial mesogen angles. Bladon et al. [50] demonstrated an entirely new nematic phase transition and showed that the shear was related to the internal nematic direction during its rotation. Due to the elastic interaction between the liquid crystal mesogens, the initial mesogen angle plays an important role in the shearing behavior of the nematic elastomer film under uniaxial tension.

Despite the intensive studies of the inflation-induced deformation of the nematic elastomer balloon, there has been far less research on the light-driven deformation behaviors. The nematic elastomer balloon may present axial contraction/expansion and twisting behaviors under the actuation of light, and has potential applications for accurate active control in the fields of soft machines and equipment, due to the huge advantages of being accurate, fast, untethered, and environmentally sustainable without chemical byproducts. Based on the experimental results of light-activated deformation of nematic elastomers, this paper proposes a phenomenological relationship between the light intensity and the light-dependent material parameter describing the polymer backbone anisotropy. Then, we establish a new theoretical model of optically-responsive nematic elastomer combined with the free energy proposed by Bladon et al. [50] and theoretically study the light-activated deformation of a nematic balloon with axial load.

This paper is written as follows. Firstly, we formulate the governing equations for the deformation of the cylindrical nematic elastomer balloon in Section 2. Secondly, the light-activated elongation/shortening and twisting behaviors under free-standing case are revealed and their mechanisms are elucidated in Section 3. Thirdly, we focus on three kinds of light-activated deformation behaviors under axial-loading case in Section 4. Finally, the conclusion of this paper is summarized.

2. Modelling of an Optically-Responsive Nematic Elastomer Balloon

Figure 1 sketches a cylindrical nematic elastomer balloon subjected to external axial load T and internal inflating pressure P under illumination with light intensity. The cylindrical balloon is made of nematic elastomer combing mesogens and polymer network in molecular scale, which is synthesized through a two-step crosslinking polymerization method [15,49]. Through incorporating photoactive molecules into nematic liquid crystal elastomers, photoactive nematic elastomers can deform when illuminated. To formulate the governing equations of the light-activated deformation and reveal its mechanism, we set the stress-free state as the reference state, in which the length of the nematic elastomer balloon is L, the cross-section diameter is D, the thickness is H, the volume is V_0, and the

initial mesogen angle is ϕ_0. In the current state, the nematic balloon is subjected to inflating pressure P, axial load T and light intensity I. The length becomes l, the cross-section diameter becomes d, the thickness becomes h, the volume changes to v, and the mesogen angle is ϕ. Due to the rotation of the liquid crystal mesogens, the upper and lower end faces of the balloon rotate relative to each other and the balloon shears with shearing angle α. For simplicity, we assume that the balloon length is much larger than the cross-section diameter, so the end effect can be ignored. In addition, the cross-section diameter is assumed to be larger than its thickness, and membrane assumption is applied. Therefore, the nematic elastomer balloon is in a homogeneous state.

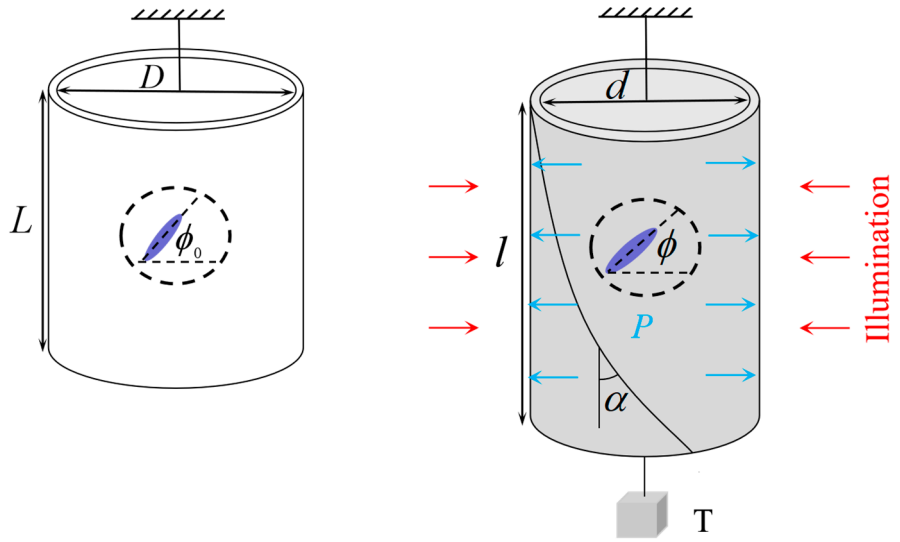

(a) Reference state (b) Current state

Figure 1. A cylindrical nematic elastomer balloon subjected to external axial load T and internal inflating pressure P under illumination with light intensity.

2.1. Governing Equations for the Light-Activated Deformation Behaviors of a Nematic Elastomer Balloon

To understand the light-activated deformation behaviors of the nematic elastomer balloon, we can derive the governing equations according to the well-known nematic elastomer theory proposed by Bladon et al. [50]. The function of the free energy density can be given as

$$W(\mathbf{F},\theta) = \frac{\mu}{2}\mathrm{tr}\left(\mathbf{l}_0\mathbf{F}^T\mathbf{l}^{-1}\mathbf{F}\right) \tag{1}$$

where μ is the shear modulus and $\mathbf{F}$ is the deformation gradient tensor in the nematic balloon, which can be written as [51–53]

$$F = \begin{bmatrix} \lambda_z & 0 & 0 \\ \lambda_z \tan\alpha & \lambda_\theta & \\ 0 & 0 & \lambda_r \end{bmatrix} \tag{2}$$

where λ_z,λ_θ and λ_r are extension ratios as follows:

$$\lambda_z = l/L,\ \lambda_\theta = d/D,\ \lambda_r = h/H \tag{3}$$

We assume that the nematic elastomer is incompressible during the deformation of the balloon, namely,

$$\lambda_\theta\lambda_z\lambda_r = 1 \tag{4}$$

$\mathbf{l}_0$ and $\mathbf{l}$ are the polymer chain configurations of the nematic elastomer before and after deformation, which can be represented by

$$\mathbf{l}_0 = \boldsymbol{\delta} + (r-1)\mathbf{n}_0\mathbf{n}_0 \tag{5}$$

And

$$\mathbf{l} = \boldsymbol{\delta} + (r-1)\mathbf{n}\mathbf{n} \tag{6}$$

where $\boldsymbol{\delta}$ is the unit tensor, r is the specific material parameter which will be given in detail in Section 2.2, and its value depends on the light intensity. $\mathbf{n}_0$ and $\mathbf{n}$ are the initial and current mesogen directors before and after deformation, which can be written as

$$\mathbf{n}_0 = (\sin\phi_0, -\cos\phi_0, 0) \tag{7}$$

And

$$\mathbf{n} = (\sin\phi, -\cos\phi, 0) \tag{8}$$

where ϕ_0 and ϕ are the initial and current mesogen angles between the mesogens and the axis of the balloon. Hence, it is found that the free energy of the nematic elastomer is affected by the above four independent parameters as $W = W(\lambda_\theta, \lambda_z, \alpha, \phi)$. In addition, during the deformation of the nematic balloon, the equilibrium equation can be given according to the second law of thermodynamics at a constant temperature as follows:

$$\delta W - s_{iK}\delta F_{iK} = 0 \tag{9}$$

where s_{iK} is the nominal stress applied on the elastomer, δW and δF_{iK} are infinitesimal variations of free energy of the elastomer and the deformation gradient. Considering that the non-zero components of nominal stress are $s_{\theta\theta}$ and s_{zz}, the Equation (9) can be written as

$$\frac{\partial W}{\partial \lambda_\theta}\delta\lambda_\theta + \frac{\partial W}{\partial \lambda_z}\delta\lambda_z + \frac{\partial W}{\partial \alpha}\delta\alpha + \frac{\partial W}{\partial \varphi}\delta\phi - s_{\theta\theta}\delta\lambda_\theta - s_{zz}\delta\lambda_z = 0 \tag{10}$$

The equilibrium equation can be further obtained that

$$\frac{\partial W(\lambda_\theta, \lambda_z, \phi, \alpha)}{\partial \lambda_\theta} = s_{\theta\theta} \tag{11}$$

$$\frac{\partial W(\lambda_\theta, \lambda_z, \phi, \alpha)}{\partial \lambda_z} = s_{zz} \tag{12}$$

$$\frac{\partial W(\lambda_\theta, \lambda_z, \phi, \alpha)}{\partial \phi} = 0 \tag{13}$$

$$\frac{\partial W(\lambda_\theta, \lambda_z, \phi, \alpha)}{\partial \alpha} = 0 \tag{14}$$

The radial stress can be ignored due to the thickness of the balloon being much smaller than the cross-section diameter. The balance of axial and hoop stresses can be expressed as

$$\sigma_{\theta\theta} = \frac{Pd}{2h}, \sigma_{zz} = \frac{Pd}{4h} + \frac{T}{\pi dh} \tag{15}$$

$$s_{\theta\theta} = \frac{PD}{2H}\lambda_\theta\lambda_z, s_{zz} = \frac{PD}{4H}\lambda_\theta^2 + \frac{T}{\pi D\mathrm{H}} \tag{16}$$

To nondimensionalize the governing equations above, we introduce the following dimensionless quantities $\overline{P} = \frac{PD}{\mu H}$ and $\overline{T} = \frac{2T}{\pi\mu D\mathrm{H}}$. A combination of Equations (1), (11)–(14)

and (16) gives the governing equations for the light-activated deformation behaviors of the balloon:

$$\overline{P}\lambda_\theta\lambda_z = \frac{2\left(r\cos^2\phi_0+\sin^2\phi_0\right)\left(r\sin^2\phi+\cos^2\phi\right)}{r}\lambda_\theta - \frac{(r-1)^2\sin(2\phi)+2(r-1)\tan\alpha\left(r\sin^2\phi+\cos^2\phi\right)}{2r}\sin(2\phi_0)\lambda_z - \frac{2}{\lambda_z^2\lambda_\theta^3} \tag{17}$$

$$\frac{\overline{P}}{2}\lambda_\theta^2 + \overline{T} = \frac{\left(r\sin^2\phi_0+\cos^2\phi_0\right)[(r-1)\cos(2\alpha-2\phi)+r+1]}{r\cos^2\alpha}\lambda_z - \frac{(r-1)\sin(2\phi_0)[(r+1)\sin\alpha+(r-1)\sin(2\phi-\alpha)]}{2r\cos\alpha}\lambda_\theta - \frac{2}{\lambda_z^3\lambda_\theta^2} \tag{18}$$

$$\frac{\left(r\sin^2\phi_0+\cos^2\phi_0\right)\sin(2\alpha-2\phi)}{\cos^2\alpha\left(r\cos^2\phi_0+\sin^2\phi_0\right)}\lambda_z^2 - \frac{(r-1)\sin(2\phi_0)\cos(2\phi-\alpha)}{\cos\alpha\left(r\cos^2\phi_0+\sin^2\phi_0\right)}\lambda_z\lambda_\theta + \sin(2\phi)\lambda_\theta^2 = 0 \tag{19}$$

$$\frac{\left(r\sin^2\phi_0+\cos^2\phi_0\right)[(r-1)\sin(2\phi-\alpha)+(r+1)\sin\alpha]}{\cos\alpha\left(r\sin^2\phi+\cos^2\phi\right)}\lambda_z - (r-1)\sin(2\phi_0)\lambda_\theta = 0 \tag{20}$$

The above formula can predict the light-activated deformation of the nematic elastomer balloon, but the relationship between the material parameter r and the light intensity is required, which will be further discussed as follows.

2.2. Light-Dependent Material Parameter r

Experiments show that the deformation of the nematic elastomer depends on the light intensity [34–37]. To explore the light-activated deformation of the nematic elastomer balloon, we need to establish the relationship between light intensity I and the material parameter describing the polymer backbone anisotropy r. For example, the typical value of parameter r is $r_L = 5.26$ without light illumination in the experiments [15,49]. When the light is infinite and the polymer backbone becomes isotropic, i.e., $r = 1$. Based on the experiments, we propose the following phenomenological relationship:

$$r = 1+(r_L-1)\mathrm{e}^{-\overline{I}} \tag{21}$$

where $\overline{I} = I/I_0$ with I_0 being characteristic light intensity. As shown in the Figure 2, with the increase of light intensity, the material parameter r gradually decreases from r_L to 1. This means that the degree of anisotropy of the polymer backbone gradually decreases to isotropy, thus causing deformation of the balloon.

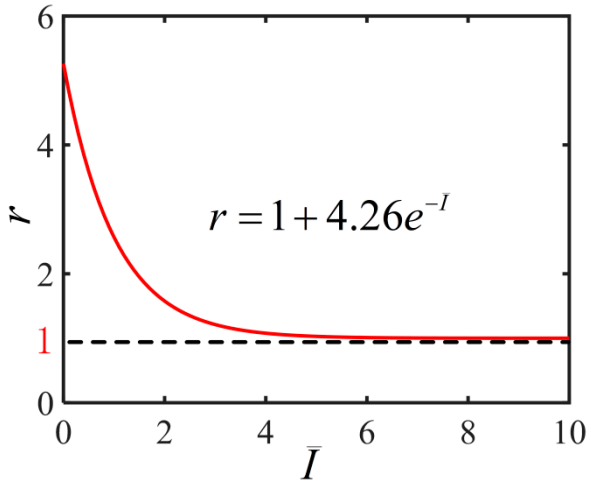

Figure 2. Variation of the light-dependent material parameter r with the light intensity $\overline{I}$ for the cylindrical nematic elastomer balloon subjected to illumination.

2.3. Solution Method

To understand the light-activated deformation behaviors of the nematic elastomer balloon, we can derive the solution of the governing Equations (17)–(21) numerically using MATLAB software. The typical values of material properties and geometric parameters from accessible experiments [15,23,48,49] are listed in Table 1, and the dimensionless parameters are estimated as $\overline{I} = 0 \sim 6$ and $\overline{T} = 0 \sim 1$. Hereon, we firstly provide the quantities such as light intensity $\overline{I}$, axial load $\overline{T}$, initial mesogen angle ϕ_0, hoop stretch λ_θ, and then we can solve the value of the axial stretch λ_z, pressure $\overline{P}$, shearing angle α, and mesogen angle ϕ in the deformed nematic balloon. Hence, the relationships between the variation of each quantity with the volume for different light intensities $\overline{I}$ in the inflation process are further drawn. Furthermore, the relationships between different physical quantities and light intensity are found for a given quantity of inflating gas. We assume that the thickness of the balloon is much thinner than the decay length of light in the nematic elastomer, such that the light intensity is homogeneous. Assuming that the gas inside the balloon is the ideal gas, its equation of state is $PV = nRT$, where $V = \frac{\pi D^2}{4} L\lambda_\theta^2\lambda_z$ is gas volume, n is quantity of inflating gas, R is ideal gas constant, and T is the thermodynamic temperature of the ideal gas. By introducing $\overline{P} = \frac{PD}{\mu H}$, $\overline{V} = \lambda_\theta^2\lambda_z$ and $\overline{n} = \frac{4nRT}{u\pi HD}$, the dimensionless form is $\overline{PV} = \overline{n}$.

Table 1. Material properties and geometric parameters.

Parameter	Definition	Value	Units
T	axial load	0~10	N
P	inflating pressure	0~100	kPa
L	the length of the balloon	100	mm
D	the cross-section diameter	10	mm
H	the thickness	1	mm
ϕ_0	initial mesogen angle	0~90	°
I	light intensity	0~10,000	W/m^2
r	Light-dependent material parameter	1~5.26	-
μ	shear modulus	0.7	MPa

In the process of solving nonlinear governing equations, we find that there are multiple solutions as shown in the Figure 3, which plots the variation of inflating pressure with the volume for $\overline{T} = 0.15$ and $\phi_0 = 45°$. Here, we briefly introduce the solution method as previously described by Li et al. [23]. The stable solution is according to the smaller potential energy of the multiple equilibrium states [23]. The blue curve in Figure 3 shows the solution of $\phi = 90°$ and the red curve shows the solution of $\phi = 0°$. In addition, the inflating pressure exhibits up/down/up/down behavior with the volume which represents a typical inflation process as shown by the black curve. The previous research shows that a bifurcation condition is valid by Maxwell's equal-area rule and the localized bulging in an inflated cylindrical balloon can take place [23–26]. There is an inhomogeneous and complex state during the localized bulging in the balloon. In the following discussion, we skip the details of the localized bulging and bulge propagation to investigate the light-activated deformation behaviors based on homogeneous analysis by assuming that the film is uniformly deformed.

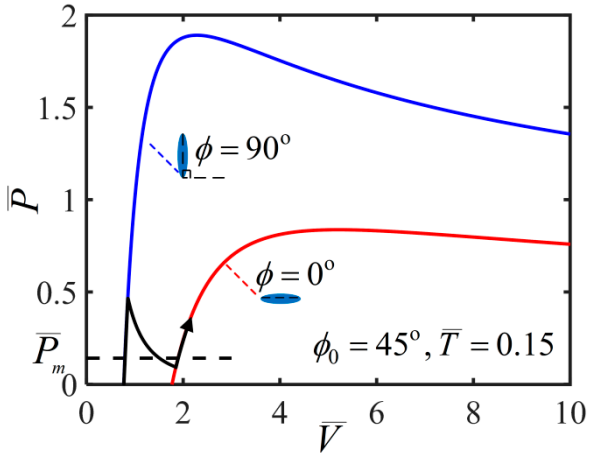

Figure 3. Pressure vs. volume during the inflation process for $\overline{T} = 0.15$ and $\phi_0 = 45°$, in which the blue curve shows the solution of $\phi = 90°$ and the red curve shows the solution of $\phi = 0°$. The black N-shaped curve shows a typical inflation process by volume control.

3. Light-Activated Contraction and Twisting of a Free-Standing Nematic Elastomer Balloon

To investigate light-activated deformation behaviors of the cylindrical free-standing nematic elastomer balloon under illumination, we first plot the variations of various physical quantities including $\overline{PV}$ (i.e., the quantity $\overline{n}$ of inflating gas), hoop stretch λ_θ, axial stretch λ_z and shearing angle α with the volume in the inflation process for initial mesogen angle $\phi_0 = 45°$ under different light intensities $\overline{I}$, as shown in Figure 4. Figure 4a shows that with the increase of the volume, the quantity $\overline{PV}$ keeps at zero. As the volume increases further, $\overline{PV}$ increases sharply when the volume exceeds a critical value $\overline{V}_{\text{crit}}$, and this typical inflating process is similar to the reported experiments [15]. Meanwhile, $\overline{V}_{\text{crit}}$ decreases with the increase of the light intensity. Figure 4b shows that with the increase of the volume, the shearing angle increases monotonously, and gradually approaches an asymptotic angle α_{asym}. With the increase of light intensity, α_{asym} decreases asymptotically to zero.

Figure 4c,d show that for a given light intensity, the radius of balloon initially increases significantly, while the length of the balloon decreases significantly. This inflation-induced axial contraction is consistent with the reported experiments [15], which is far different from the case of routine balloons [19–22]. During the further inflation process, both the radius and length of the balloon increase, and the mesogen angle becomes locked at 0°, as shown in Figure 5 plotting the variation of mesogen angle with the volume during the inflation process. With the increase of light intensity, the radius decreases while the length increases.

Based on the results of various physical quantities during the inflation process, we further analyze the light-activated deformation behaviors of the free-standing nematic elastomer balloon for the different initial angles under a constant quantity of inflating gas. Figure 6a,b plot the variations of hoop stretch λ_θ and axial stretch λ_z with the light intensity for different initial mesogen angles. For $\phi_0 = 0°$, both the radius and length of the balloon remain unchanged with the increase of the light intensity. For nonzero initial mesogen angle, the radius of the non-illuminated balloon has an initial value due to the inflation, which increases with the increase of the initial mesogen angle ϕ_0. For a given nonzero initial mesogen angle, the radius gradually decreases to 1 with the increase of light intensity (Figure 6a). The length of non-illuminated balloon also has an initial value due to the inflation, which decreases with the increase of ϕ_0. For a given initial mesogen angle, the length increases gradually to 1 with the increase of light intensity (Figure 6b).

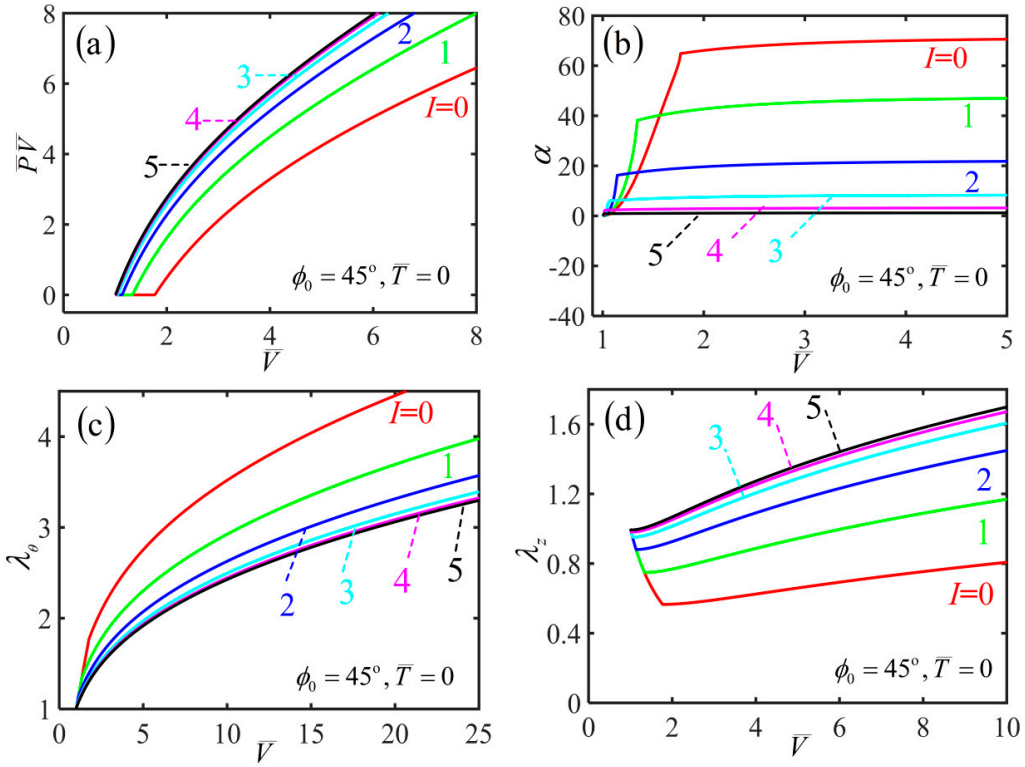

Figure 4. Variation of (**a**) $\overline{PV}$, (**b**) shearing angle, (**c**) hoop stretch and (**d**) axial stretch with the volume during the inflation process of a free-standing nematic elastomer balloon for different light intensities.

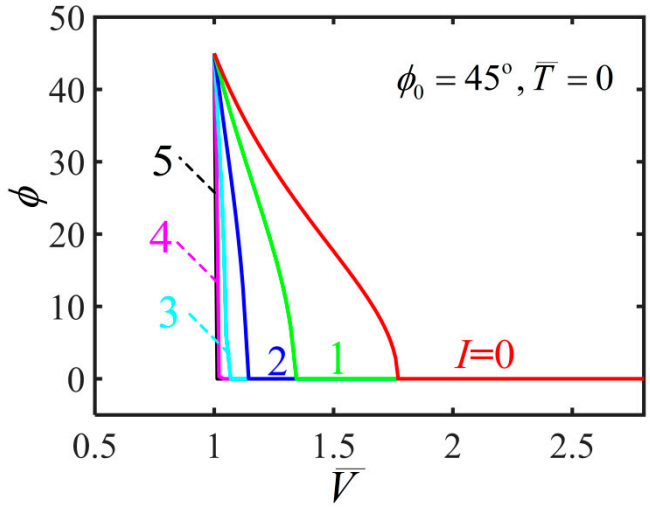

Figure 5. The variation of mesogen angle with the volume during the inflation process of a free-standing nematic elastomer balloon for different light intensities.

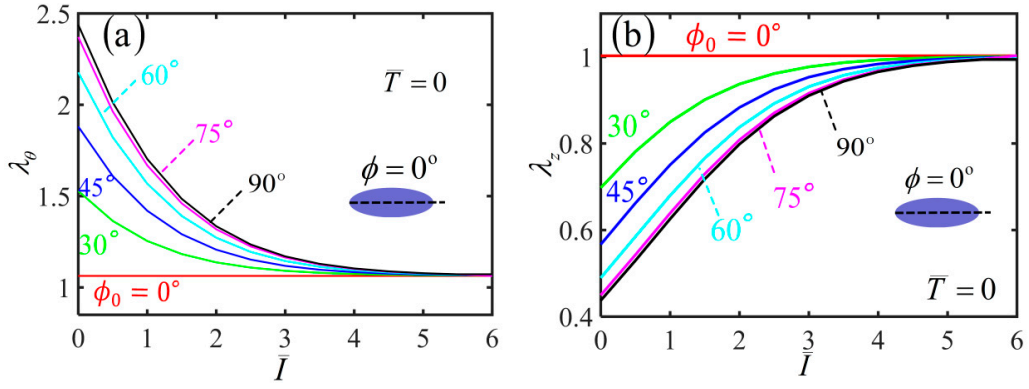

Figure 6. Variations of (**a**) hoop stretch and (**b**) axial stretch with the light intensity of the free-standing nematic elastomer balloon for different initial mesogen angles.

Figure 7 plots the variation of shearing angle with the light intensity for different initial mesogen angles. For $\phi_0 = 0°$ and $\phi_0 = 90°$, the shearing angle of the balloon is always kept at $0°$ with the increase of the light intensity. For $0 < \phi_0 < 90°$, the shearing angle monotonously decreases with the increase of light intensity. For a given light intensity, the shearing angle firstly increases and then decreases with the increase of the initial mesogen angle, which has the maximum at $\phi_0 = 45°$. Meanwhile, for a light intensity large enough, the balloon does not shear in the membrane, and the upper and lower end cross-sections do not twist. This is because the material parameter r is close to 1 and the polymer backbone becomes isotropic.

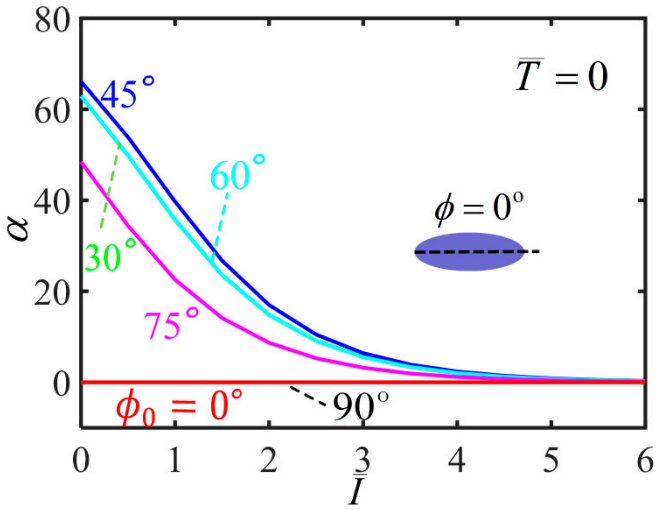

Figure 7. Variations of shearing angle α with the light intensity of the free-standing nematic elastomer balloon for different initial mesogen angles.

In order to understand the light-activated deformation process of the balloon, Figure 8 illustrates a typical process of a free-standing nematic elastomer balloon for an initial mesogen angle $\phi_0 = 45°$ under different light intensities. From the reference state to the initial non-illuminated state, the radius of balloon increases significantly while the length decreases significantly, which is consistent with the reported experiments [15]. Meanwhile, the mesogen angle ϕ becomes locked at $0°$. With the increase of light intensity, the radius decreases close to 1, while the length increases close to 1. The mesogen angle keeps at $0°$ and is not affected by illumination. The shearing angle α monotonously decreases with the increase of light intensity.

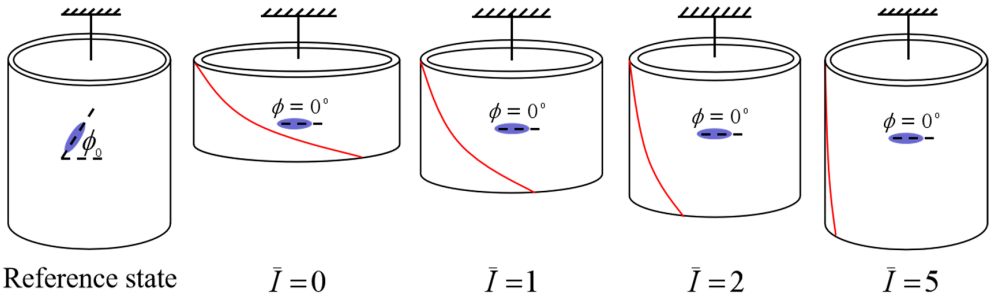

Figure 8. The representative process of a free-standing nematic elastomer balloon for initial mesogen angle $\phi_0 = 45°$ under different light intensities.

4. Light-Activated Contraction and Twisting of a Nematic Elastomer Balloon Subjected to External Axial Load

He et al. [15] experimentally studied the inflation behavior of the nematic balloon when it is subjected to an additional axial load. It was found that the axial load represented an important factor associated with the inflation of elastomer balloons. To study the light-activated deformation behaviors of cylindrical nematic balloon with an additional axial load under illumination, we first plot the variations of various physical quantities with the volume in the inflation process for initial mesogen angle $\phi_0 = 45°$ and axial load $\overline{T} = 0.1$ under different light intensities $\bar{I}$, as shown in Figure 9. Figure 9a shows that the curve is N-shaped, indicating the balloon initially shrinks conspicuously in volume with the additional axial load, and this typical inflating process is similar to the reported experiments [15]. It is an anomalous phenomenon, which is far different from the free-standing state of nematic elastomer balloon, and can be explained with the soft elasticity or zero energy mode deformation [50]. Meanwhile, there is an inhomogeneous and complex state during the localized bulge formation and propagation in the balloon [23–26]. After the whole balloon is bulged, the $\overline{PV}$ increases with the increasing volume, and the mesogen angle is kept at 0°.

Figure 9b shows that, for a given light intensity, the shear angle of the balloon initially decreases, then increases gradually to an asymptotic angle with the inflating air amount increasing. With the increase of inflating air volume, the shearing angle finally gradually approaches an asymptotic value, which decreases with the increase of light intensity. Figure 9c shows that for a given light intensity, there is an obvious initial shortening in the hoop direction of the balloon, and then the hoop stretch increases with the subsequent inflation process. Figure 9d shows that for a given light intensity, the balloon exhibits conspicuous initial elongation in the axial direction. During the subsequent inflation process, the length firstly decreases and then increases with the increase of volume. The results are consistent with the reported experiments [15].

Based on the results of various physical quantities in the inflation process and the N-shaped curve shown in Figure 9a, it is found that the balloon bears three kinds of light-activated deformation behaviors for different initial mesogen angles, which depend on the constant quantity of inflating gas.

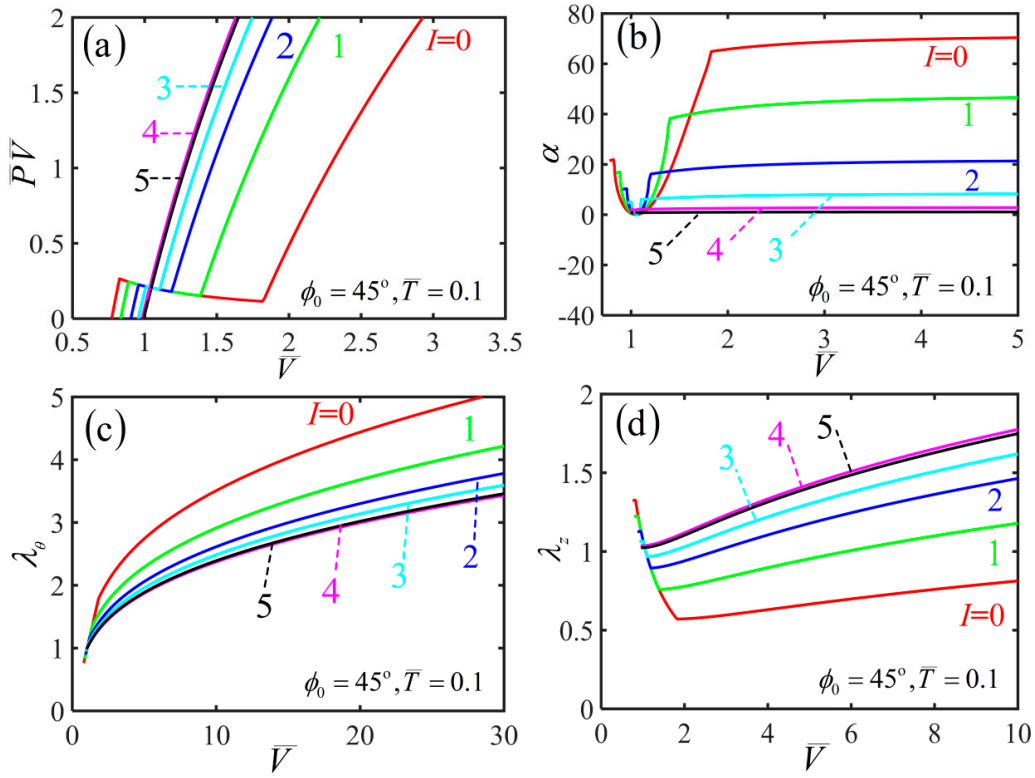

Figure 9. Variations of (**a**) $\overline{PV}$, (**b**) shearing angle, (**c**) hoop stretch and (**d**) axial stretch with the volume of the nematic elastomer balloon subjected to axial load $\overline{T} = 0.1$ and mesogen angle $\phi_0 = 45°$ for different light intensities.

(1) The case of small PV

For a small quantity of inflating gas, Figure 10 plots the variations of hoop stretch λ_θ and axial stretch λ_z with the light intensity for different initial mesogen angles. For $\phi_0 = 0°$, both the radius and length of the balloon remain unchanged with the increase of light intensity. For a nonzero initial mesogen angle, the radius of the non-illuminated balloon has an initial value due to the inflation, which increases with the increasing initial mesogen angle. For a given nonzero initial mesogen angle, the radius gradually increases to 1 with the increase of light intensity (Figure 10a). Moreover, the length of non-illuminated balloon also has an initial value due to the inflation, which decreases with the increase of ϕ_0. For a given initial mesogen angle, the length decreases gradually to 1 with the increase of light intensity (Figure 10b).

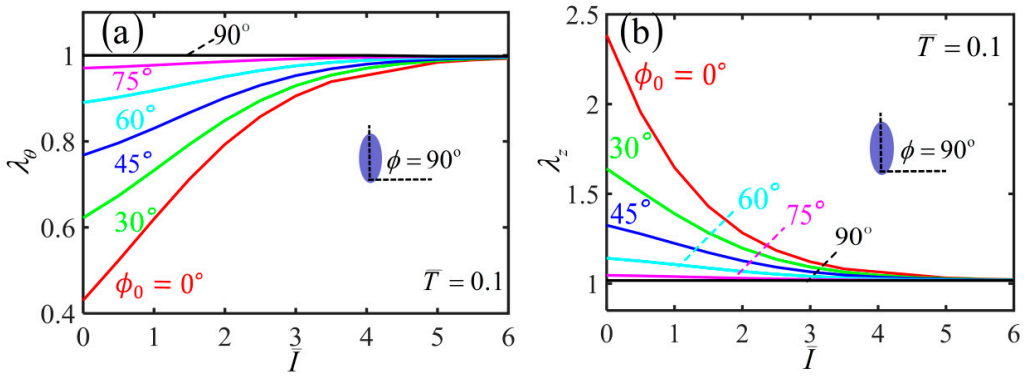

Figure 10. Variation of (**a**) hoop stretch and (**b**) axial stretch with the light intensity of the nematic elastomer balloon with axial load $\overline{T} = 0.1$ for different initial mesogen angles.

Figure 11 plots the variation of the shearing angle α with the light intensity for different initial mesogen angles. For a given light intensity, the shearing angle firstly increases and then decreases with the increase of the initial mesogen angle, which has the maximum at $\phi_0 = 45°$. For $\phi_0 = 0°$ and $\phi_0 = 90°$, the shearing angle of the balloon is always kept at $0°$ with the increase of the light intensity. For $0 < \phi_0 < 90°$, the shearing angle monotonously decreases to 0 with the increase of light intensity. For infinite light intensity, the balloon does not twist because the polymer backbone becomes isotropic.

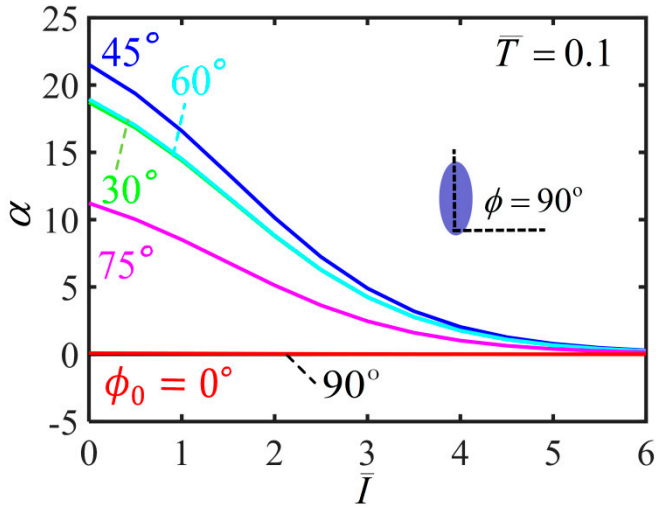

Figure 11. Variation of the shearing angle with the light intensity of the nematic elastomer balloon with axial load $\bar{T} = 0.1$ for different initial mesogen angles.

Figure 12 illustrates a typical process of a nematic elastomer balloon for initial mesogen angle $\phi_0 = 45°$ and axial load $\bar{T} = 0.1$. From the reference state to the initial non-illuminated state, the radius of the balloon initially decreases significantly while the length of balloon increases significantly, and the mesogen angle becomes locked at 90°, which is consistent with the reported experiments [15]. With the increase of light intensity, the radius increases and the length decrease asymptotically to 1. The mesogen angle keeps at 90° and is not affected by the light illumination. The shearing angle monotonously decreases with the increase of light intensity.

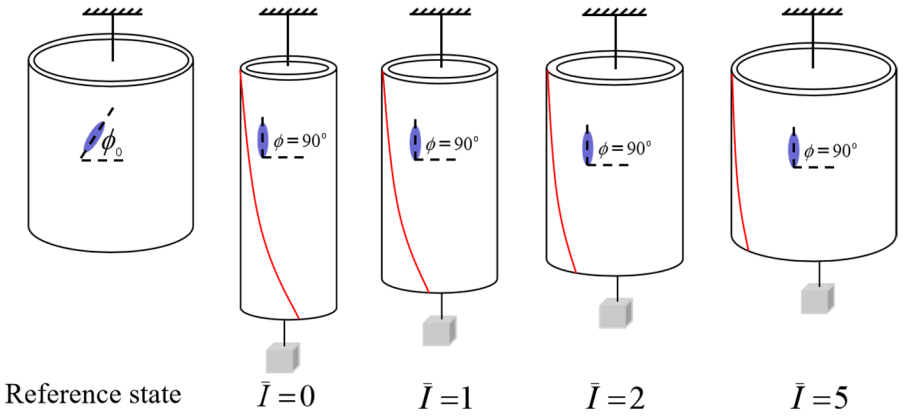

Figure 12. The representative process of a nematic elastomer balloon for initial mesogen angle $\phi_0 = 45°$ and axial load $\bar{T} = 0.1$ under different light intensities.

(2) The case of medium PV

For a medium quantity of inflating gas, the light-activated deformation of the balloon may accompany the complex process of localized bulging and bulge propagation. The

localized bulging balloon is in an inhomogeneous two-phase coexisting state, which is beyond the research scope of this paper. Based on our homogeneous state-based model, we focus on the phase transition between homogeneous and inhomogeneous states in the process of light-activated deformation.

Figure 13 dedicates the relationship of the value of $\overline{PV}$ (i.e., the quantity of inflating gas) and the volume in the inflating process of a nematic elastomer balloon for $\overline{T} = 0.1$ and $\phi_0 = 45°$ under different light intensities. The dotted lines represent Maxwell's condition for the coexistence of two phases [23–26]. For a given medium quantity of inflating gas, an initial state A with $\overline{I} = 0$ is lower than the red dotted line of its own Maxwell states and is in localized bulging state. With the increase of light intensity, the state moves along the horizontal arrow line due to constant quantity of the inflating gas. With the further increase of the light intensity, the state can move from A to B, which is higher than the blue dotted line of its own Maxwell states and is in the wholly-bulged state. It is concluded that increasing the light intensity can promote bulge propagation, and enables phase transition between homogeneous and inhomogeneous states. In addition, for a given small or large quantity of inflating gas, the balloon without illumination is initially in a homogeneous unbulged state (e.g., state C or E in Figure 13). With the increase of light intensity, the state changes without bulging and phase transition (e.g., from C to D or E to F), in which the deformation of the balloon can be predicted by our homogeneous state-based model.

With the decrease of the light intensity, for a given small or large quantity of inflating gas, the state similarly changes without bulging and phase transition (e.g., from D to C or F to E). However, for given medium quantity of inflating gas, with the decrease of light intensity, an initial wholly-bulged state B can change to locally-bulged state A, or an initial bulged state G can change to another bulged state H. Different from the case of increasing light intensity, the balloon may always be in a bulged state.

Figure 14 presents a typical schematic diagram for the light-activated deformation accompanied with the localized bulging and bulge propagation of the cylindrical nematic elastomer balloon. For an initial localized bulging non-illuminated state, with the increase of light intensity, the bulge propagates and the balloon can be wholly bulged finally, which shows the phase transition between homogeneous and inhomogeneous states in the process of light-activated deformation.

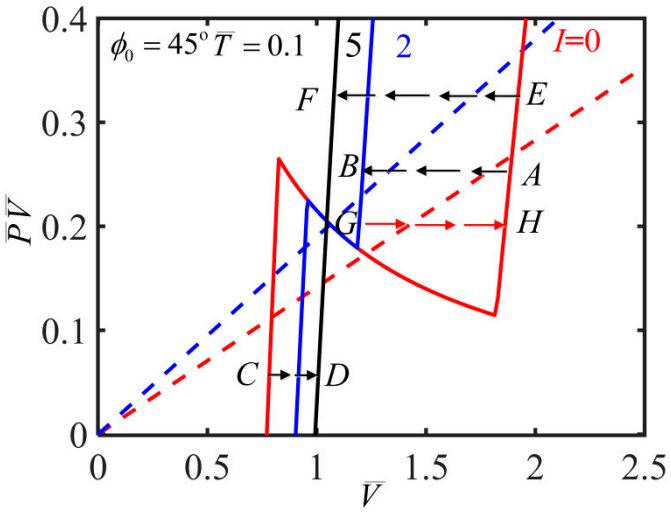

Figure 13. Variations of $\overline{PV}$ versus volume of the balloon under different light intensities with initial mesogen angle $\phi_0 = 45°$ and axial load $\overline{T} = 0.1$.

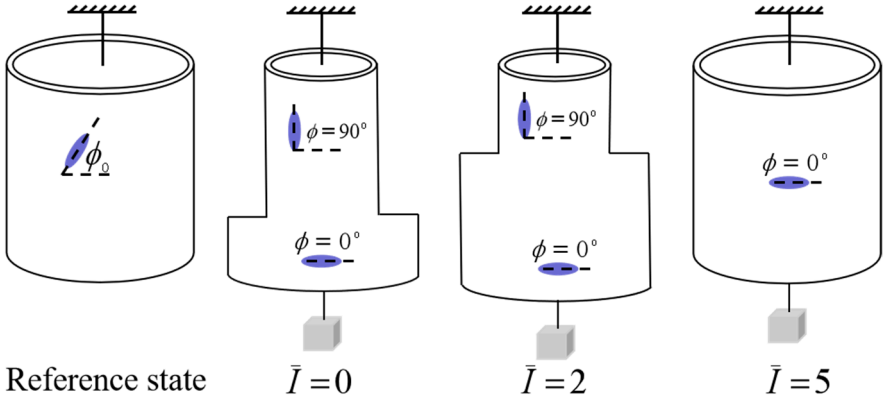

Figure 14. The representative process of a nematic elastomer balloon for initial mesogen angle $\phi_0 = 45°$ and axial load $\overline{T} = 0.1$ under different light intensities.

(3) The case of large PV

For a large quantity of inflating gas, the light-activated deformation behaviors of the balloon are similar to the case of the free-standing balloon in Section 3. For $\phi_0 = 0°$, both the radius and length of the balloon remain unchanged with the increase of the light intensity. For a nonzero initial mesogen angle, the radius of the non-illuminated balloon has an initial value due to the inflation, which increases with the increase of the initial mesogen angle ϕ_0. For a given nonzero initial mesogen angle, the radius gradually decreases to 1 with the increase of light intensity (Figure 15a). The length of non-illuminated balloon also has an initial value due to the inflation, which decreases with the increase of ϕ_0. For a given initial mesogen angle, the length increases gradually to 1 with the increase of light intensity (Figure 15b).

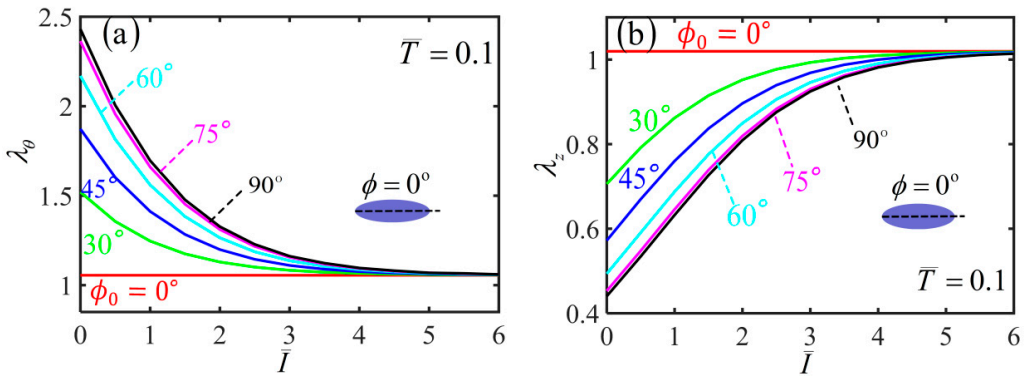

Figure 15. Variations of (**a**) hoop stretch and (**b**) axial stretch with the light intensity of the nematic elastomer balloon with axial load $\overline{T} = 0.1$ for different initial mesogen angles.

Figure 16 plots the variation of shearing angle with the light intensity during inflation process for different initial mesogen angles. For a given light intensity, the shearing angle firstly increases and then decreases with the increase of the initial mesogen angle, which has the maximum at $\phi_0 = 45°$. For $\phi_0 = 0°$ and $\phi_0 = 90°$, the shearing angle of the balloon is always kept at 0° with the increase of the light intensity. For $0 < \phi_0 < 90°$, the shearing angle monotonously decreases to 0 with increasing light intensity. For infinite light intensity, the balloon does not twist because the polymer backbone becomes isotropic.

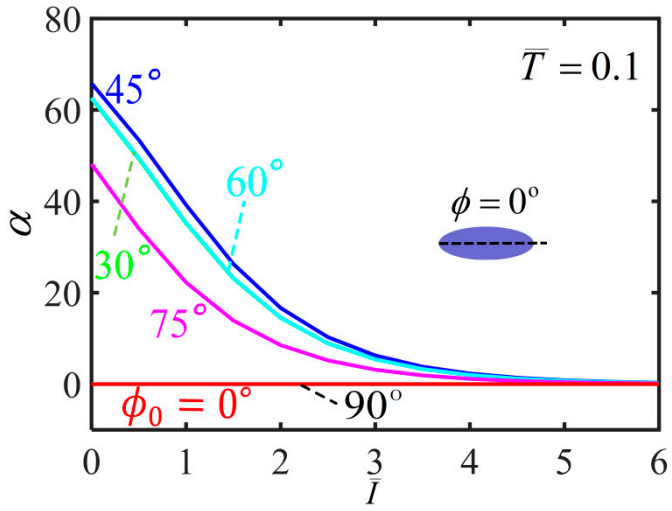

Figure 16. Variations of shearing angle α with the light intensity of the nematic elastomer balloon with axial load $\overline{T} = 0.1$ for different initial mesogen angles.

Figure 17 illustrates a typical process of a nematic elastomer balloon for initial mesogen angle $\phi_0 = 45°$ and axial load $\overline{T} = 0.1$. From the reference state to the initial non-illuminated state, the radius of balloon initially increases significantly while the length of the balloon decreases significantly, and the mesogen angle becomes locked at 0°, which is consistent with the reported experiments [15]. With the increase of light intensity, the radius decreases and the length increases asymptotically to 1. The mesogen angle keeps at 0° and is not affected by the light illumination. The shearing angle monotonously decreases with the increase of light intensity.

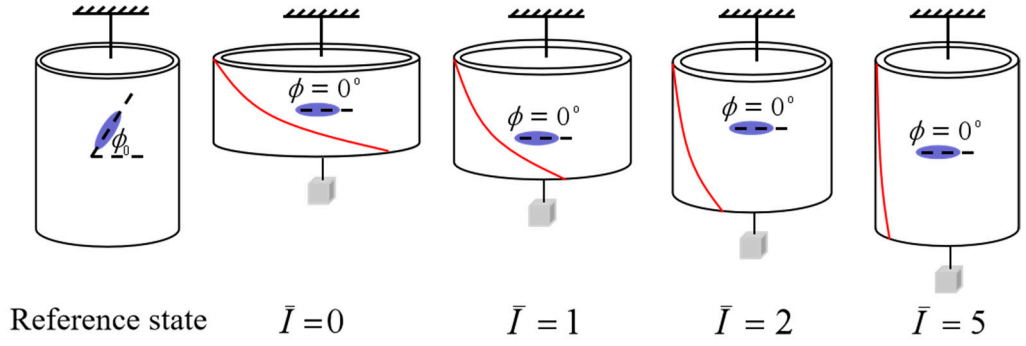

Figure 17. The representative process of a nematic elastomer balloon for initial mesogen angle $\phi_0 = 45°$ and axial load $\overline{T} = 0.1$ under different light intensities.

5. Conclusions

Based on experimental results of light-activated deformation of nematic elastomers, we propose a phenomenological relationship between the light intensity and the material parameter r describing the polymer backbone anisotropy. Then, a new theoretical model of optically-responsive nematic elastomer is further established to investigate the light-activated elongation/shortening and twisting behaviors of a cylindrical nematic elastomer balloon. For the free-standing balloon, the light-activated expansion and twisting behaviors are presented and the mechanism is elucidated. For the balloon subjected to a constant axial load, three kinds of light-activated deformation behaviors are investigated. The light intensity and the initial mesogen angle greatly affect the hoop stretch, the axial stretch, the shearing angle and the mesogen angle of the nematic elastomer balloon. In the future, a theoretical model based on an inhomogeneous state needs to be further established to study the bulging of the nematic elastomer balloon. In addition, the deformation behavior

of balloon actuators under external torque and torsional restraint deserves to be further explored. It is expected that our results will deepen the understanding of light-activated deformation of the nematic elastomer balloon, and provide guidance for its potential applications in light-activated actuators and machines.

Author Contributions: The contribution of the authors are as follows: Conceptualization, Methodology, Writing—Original draft preparation, L.Z.; software, validation, Y.W.; Writing—Review and editing, supervision, K.L. All authors have read and agreed to the published version of the manuscript.

Funding: KL acknowledges the supports from National Natural Science Foundation of China (Grant No. 12172001), Outstanding Talents Cultivation Project of Universities in Anhui (Grant No. gxyqZD2019056) and University Natural Science Research Project of Anhui Province (Grant No. KJ2020A0449). LZ acknowledges the support from Doctoral Startup Foundation from Anhui Jianzhu University (Grant No. 2020QDZ14).

Institutional Review Board Statement: Not applicable.

Informed Consent Statement: Not applicable.

Data Availability Statement: The data that support the findings of this study are available upon reasonable request from the authors.

Conflicts of Interest: The authors declare no conflict of interest.

References

1. Finkelmann, H.; Nishikawa, E.; Pereira, G.G.; Warner, M. A New Opto-Mechanical Effect in Solids. *Phys. Rev. Lett.* **2001**, *87*, 015501. [CrossRef] [PubMed]
2. Warner, M.; Terentjev, E.M. *Liquid Crystal Elastomers*; Oxford University Press: Oxford, UK, 2007.
3. Desimone, A. Energetics of fine domain structures. *Ferroelectr. Statl. Nonlinear Soft Matter Phys.* **1999**, *222*, 275–284. [CrossRef]
4. De Simone, A.; Dolzmann, G. Material instabilities in nematic elastomers. *Phys. D Nonlinear Phenom.* **2000**, *136*, 175–191. [CrossRef]
5. Finkelmann, H.; Kundler, I.; Terentjev, E.; Warner, M. Critical stripe-domain instability of nematic elas-tomers. *Journal de Physique II* **1997**, *7*, 1059–1069. [CrossRef]
6. Cesana, P.; De Simone, A. Quasiconvex envelopes of energies for nematic elastomers in the small strain regime and applications. *J. Mech. Phys. Solids* **2011**, *59*, 787–803. [CrossRef]
7. Conti, S.; De Simone, A.; Dolzmann, G. Semisoft elasticity and director reorientation in stretched sheets of nematic elastomers. *Phys. Rev. E* **2002**, *66*, 061710. [CrossRef] [PubMed]
8. Lin, P.W.; Liu, C.H. Bio-Inspired Soft Proboscis Actuator Driven by Dielectric Elastomer Fluid Transduc-ers. *Polymers* **2019**, *11*, 142. [CrossRef] [PubMed]
9. Connolly, F.; Polygerinos, P.; Walsh, C.J.; Bertoldi, K. Mechanical programming of soft actuators by vary-ing fiber angle. *Soft Robot.* **2015**, *2*, 26–32. [CrossRef]
10. Zhang, C.; Liu, L.; Xu, K.; Dong, Z.; Ding, Y.; Li, Q.; Li, P. Hydraulically Coupled Dielectric Elastomer Ac-tuators for a Bioinspired Suction Cup. *Polymers* **2021**, *13*, 3481. [CrossRef] [PubMed]
11. Shim, J.-E.; Quan, Y.-J.; Wang, W.; Rodrigue, H.; Song, S.-H.; Ahn, S.-H. A smart soft actuator using a single shape memory alloy for twisting actuation. *Smart Mater. Struct.* **2015**, *24*, 125033. [CrossRef]
12. Liu, K.; Chen, S.; Chen, F.; Zhu, X. A Unidirectional Soft Dielectric Elastomer Actuator Enabled by Built-In Honeycomb Metastructures. *Polymers* **2020**, *12*, 619. [CrossRef]
13. Yan, J.; Zhang, X.; Xu, B.; Zhao, J. A New Spiral-Type Inflatable Pure Torsional Soft Actuator. *Soft Robot.* **2018**, *5*, 527–540. [CrossRef] [PubMed]
14. Shimizu, K.; Nagai, T.; Shintake, J. Dielectric Elastomer Fiber Actuators with Aqueous Electrode. *Polymers* **2021**, *13*, 4310. [CrossRef] [PubMed]
15. He, Q.; Zheng, Y.; Wang, Z.; He, X.; Cai, S. Anomalous inflation of a nematic balloon. *J. Mech. Phys. Solids* **2020**, *142*, 104013. [CrossRef]
16. Giudici, A.; Biggins, J.S. Giant deformations and soft-inflation in LCE balloons. *EPL* **2020**, *132*, 36001. [CrossRef]
17. Heo, Y.H.; Choi, D.-S.; Kim, D.E.; Kim, S.-Y. Flexible Vibrotactile Actuator Based on Dielectric Elastomer for Smart Handheld Devices. *Appl. Sci.* **2021**, *11*, 12020. [CrossRef]
18. Fried, E.; Sellers, S. Free-energy density functions for nematic elastomers. *J. Mech. Phys. Solids* **2004**, *52*, 1671–1689. [CrossRef]
19. Mallock, A., II. Note on the instability of India-rubber tubes and balloons when distended by fluid pressure. *Proc. R. Soc. Lond.* **1891**, *49*, 458–463. [CrossRef]
20. Chater, E.; Hutchinson, J.W. On the propagation of bulges and buckles. *J. Appl. Mech.* **1984**, *51*, 269–277. [CrossRef]

21. Kyriakides, S.; Yu-Chung, C. The initiation and propagation of a localized instability in an inflated elastic tube. *Int. J. Solids Struct.* **1991**, *27*, 1085–1111. [CrossRef]
22. Lestringant, C.; Audoly, B. A diffuse interface model for the analysis of propagating bulges in cylindrical balloons. *Proc. R. Soc. A Math. Phys. Eng. Sci.* **2018**, *474*, 20180333. [CrossRef]
23. Li, K.; Wang, Q.; Xu, P. Inflation-induced torsion and bulging of a nematic elastomer balloon. *Thin-Walled Struct.* **2021**, *170*, 108621. [CrossRef]
24. Wang, S.; Guo, Z.; Zhou, L.; Li, L.; Fu, Y. An experimental study of localized bulging in inflated cylindrical tubes guided by newly emerged analytical results. *J. Mech. Phys. Solids* **2019**, *124*, 536–554. [CrossRef]
25. Fu, Y.B.; Liu, J.L.; Francisco, G.S. Localized bulging in an inflated cylindrical tube of arbitrary thick-ness-the effect of bending stiffness. *J. Mech. Phys. Solids* **2016**, *90*, 45–60. [CrossRef]
26. Liu, Y.; Ye, Y.; Althobaiti, A.; Xie, Y.-X. Prevention of localized bulging in an inflated bilayer tube. *Int. J. Mech. Sci.* **2019**, *153-154*, 359–368. [CrossRef]
27. Chen, Y.-C.; Fried, E. Uniaxial nematic elastomers: Constitutive framework and a simple application. *Proc. R. Soc. A Math. Phys. Eng. Sci.* **2006**, *462*, 1295–1314. [CrossRef]
28. Liu, Y.; Ma, W.; Dai, H.H. Bending-induced director reorientation of a nematic liquid crystal elastomer bonded to a hyperelastic substrate. *J. Appl. Phys.* **2021**, *129*, 104701. [CrossRef]
29. Liu, Y.; Ma, W.; Dai, H.-H. On a consistent finite-strain plate model of nematic liquid crystal elastomers. *J. Mech. Phys. Solids* **2020**, *145*, 104169. [CrossRef]
30. Kim, T.; Zhu, L.; Al-Kaysi, R.O.; Bardeen, C.J. Organic Photomechanical Materials. *ChemPhysChem* **2014**, *15*, 400–414. [CrossRef] [PubMed]
31. Cviklinski, J.; Tajbakhsh, A.R.; Terentjev, E.M. UV isomerisation in nematic elastomers as a route to photo-mechanical transducer. *Eur. Phys. J. E* **2002**, *9*, 427–434. [CrossRef]
32. Dong, X.; Tong, F.; Hanson, K.M.; Al-Kaysi, R.O.; Kitagawa, D.; Kobatake, S.; Bardeen, C.J. Hybrid or-ganic–inorganic photon-powered actuators based on aligned diarylethene nanocrystals. *Chem. Mater.* **2019**, *31*, 1016–1022. [CrossRef]
33. Zeng, H.; Wasylczyk, P.; Wiersma, D.S.; Priimagi, A. Light robots: Bridging the gap between microrobot-ics and photomechanics in soft materials. *Adv. Mater.* **2018**, *30*, 1703554. [CrossRef] [PubMed]
34. Warner, M.; Bladon, P.; Terentjev, E.M. "Soft elasticity"-deformation without resistance in liquid crystal elastomers. *J. Phys. II* **1994**, *4*, 93–102. [CrossRef]
35. Corbett, D.; Warner, M. Linear and Nonlinear Photoinduced Deformations of Cantilevers. *Phys. Rev. Lett.* **2007**, *99*, 174302. [CrossRef] [PubMed]
36. Dunn, M.L. Photomechanics of mono- and polydomain liquid crystal elastomer films. *J. Appl. Phys.* **2007**, *102*, 013506. [CrossRef]
37. Lin, Y.; Jin, L.; Huo, Y. Quasi-soft opto-mechanical behavior of photochromic liquid crystal elastomer: Linearized stress–strain relations and finite element simulations. *Int. J. Solids Struct.* **2012**, *49*, 2668–2680. [CrossRef]
38. Kundler, I.; Finkelmann, H. Strain-induced director reorientation in nematic liquid single crystal elasto-mers. *Macromol. Rapid Comm.* **1995**, *16*, 679–686. [CrossRef]
39. Wang, Z.; Fan, W.; He, Q.; Wang, Y.; Liang, X.; Cai, S. A simple and robust way towards reversible mechanochromism: Using liquid crystal elastomer as a mask. *Extreme Mech. Lett.* **2017**, *11*, 42–48. [CrossRef]
40. Conti, S.; De Simone, A.; Dolzmann, G. Soft elastic response of stretched sheets of nematic elastomers: A numerical study. *J. Mech. Phys. Solids* **2002**, *50*, 1431–1451. [CrossRef]
41. Modes, C.D.; Bhattacharya, K.; Warner, M. Disclination-mediated thermo-optical response in nematic glass sheets. *Phys. Rev. E* **2010**, *81*, 060701. [CrossRef]
42. Stenull, O.; Lubensky, T.C. Anomalous elasticity of nematic elastomers. *Eur. Lett.* **2003**, *61*, 776–782. [CrossRef]
43. Hogan, P.M.; Tajbakhsh, A.R.; Terentjev, E.M. UV manipulation of order and macroscopic shape in ne-matic elastomers. *Phys. Rev. E* **2002**, *65*, 041720. [CrossRef] [PubMed]
44. Yu, Y.; Nakano, M.; Ikeda, T. Directed bending of a polymer film by light. *Nature* **2003**, *425*, 145. [CrossRef] [PubMed]
45. Kuenstler, A.S.; Hayward, R.C. Light-induced shape morphing of thin films. *Curr. Opin. Colloid Interface Sci.* **2019**, *40*, 70–86. [CrossRef]
46. White, T.J. Photomechanical effects in liquid crystalline polymer networks and elastomers. *J. Polym. Sci. Part B Polym. Phys.* **2018**, *56*, 695–705. [CrossRef]
47. Jin, L.; Yan, Y.; Huo, Y. A gradient model of light-induced bending in photochromic liquid crystal elasto-mer and its nonlinear behaviors. *Int. J. Non-Linear Mech.* **2010**, *45*, 370–381. [CrossRef]
48. Bai, R.; Bhattacharya, K. Photomechanical coupling in photoactive nematic elastomers. *J. Mech. Phys. Solids* **2020**, *144*, 104115. [CrossRef]
49. He, X.; Zheng, Y.; He, Q.; Cai, S. Uniaxial tension of a nematic elastomer with inclined mesogens. *Extreme Mech. Lett.* **2020**, *40*, 100936. [CrossRef]
50. Bladon, P.; Terentjev, E.M.; Warner, M. Transitions and instabilities in liquid crystal elastomers. *Phys. Rev. E* **1993**, *47*, R3838–R3840. [CrossRef]
51. Rivlin, R.S. Large elastic deformations of isotropic materials VI. Further results in the theory of torsion, shear and flexure. *Philos. Trans. R. Soc. London. Ser. A Math. Phys. Sci.* **1949**, *242*, 173–195. [CrossRef]

52. Ericksen, J.L. Deformations possible in every isotropic, incompressible, perfectly elastic body. *Zeitschrift für angewandte Mathematik und Physik* **1954**, *5*, 466–489. [CrossRef]
53. Lee, V.; Bhattacharya, K. Actuation of cylindrical nematic elastomer balloons. *J. Appl. Phys.* **2021**, *129*, 114701. [CrossRef]